in crystals may exhibit waveguiding properties, but guidance occurs only in the surrounding areas of residual stress left within the material by the laser beam passage [3]. On the other hand, by writing multiple tracks with a reduced RI around the unmodified volume of material it is possible to produce a depressed-index cladding with the central volume serving as the core of a WG [4–6, 10, 12], whereby the mechanical stress has minor influence on the WG modes. The simplest type of depressed-index cladding consists of only two parallel tracks positioned close to each other [3, 18]. But such a WG structure does not allow for control over the waveguiding properties. On the other hand, due to geometric flexibility, the depressed cladding may consist of a fairly large number of arbitrarily arranged tracks confining the flexibly large and shaped core guiding area [17]. Depressed-cladding WGs have been demonstrated to achieve light propagation with good mode confinement at different wavelengths, and low propagation losses as compared with directly written, single-track WGs [5, 6, 10, 17, 19]. It has also been proved that depressed-cladding WGs in nonlinear crystals can achieve enhanced-efficiency second-harmonic generation as compared with stress-induced WGs [20, 21].

In this paper, we study numerically depressed-cladding, buried WGs that can be formed in a *z*-cut $LiNbO_3$ crystal by fs laser writing, in a pursuit of establishing how experimentally accessible parameters, such as the number, position and size of the cladding tracks, and the RI contrast between the low-index cladding structure and the core guiding region, can be used for achieving control over the propagation constants of modes with different polarizations, hence the conditions for (quasi-) phase matching in a WG geometry. A similar approach has already been used for controlling the waveguiding properties of micro-structured optical fibres (MOFs) [22–24], where tracks with a reduced RI are naturally formed during the fibre drawing process. The results presented in this paper are relevant to various applications. These include optical parametric amplifiers with a small footprint based on WGs in $\chi^{(2)}$-nonlinear materials, ultrafast, synchronously-pumped single-photon (quantum) sources and detectors realized as WG-based, frequency-conversion modules, all-optical wavefront generators and pulse shapers, and mid-infrared (IR) integrated optical components.

2. Waveguide packing geometry and methodology

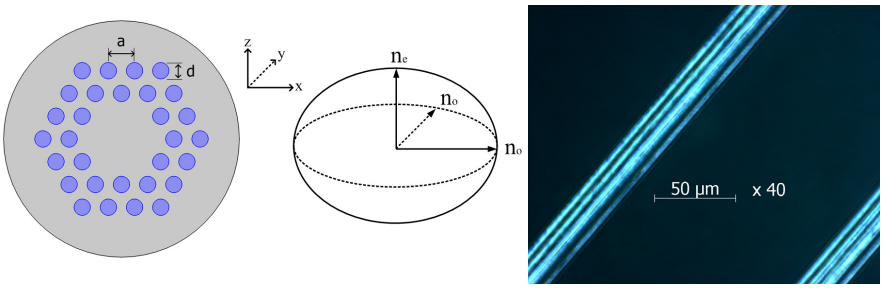

Fig. 1. Left: cross section of modeled depressed-cladding WG with two rings of tracks, and ellipsoid of indices for $LiNbO_3$ host. Right: top microscopic view of example micro-structured WG fabricated in $LiNbO_3$ by high-repetition-rate fs laser.

For this study, we modeled depressed-cladding WG structures with a hexagonal shape. This is a fairly commonly used WG shape, which has already been well studied in the case of isotropic materials such as MOFs [24]. The depressed cladding was formed by a finite number of rings of regularly spaced, cylindrical tracks whose centers were arranged hexagonally, as shown in Fig. 1. These tracks can be written in a $LiNbO_3$ crystal by direct fs laser irradiation using a transverse inscription geometry [3]. In Fig. 1 we also show the microscopic image of a top

#191696 - $15.00 USD Received 4 Jun 2013; revised 1 Jul 2013; accepted 2 Jul 2013; published 10 Jul 2013

view of an example WG that we have fabricated in $LiNbO_3$ crystal with a high-repetition-rate fs laser system, revealing smooth, high-contrast tracks, without any coloring. In our modeling, the reduced RI of the tracks was assumed to be a real value, uniform across the cross section of a track, and polarization- and wavelength-independent. Note that this might not be the case in practical scenarios, especially under arbitrary fs laser irradiation protocols. Indeed, direct measurements of the ultrafast dynamics of the dielectric permittivity of glass materials [25] revealed that irradiation by high-repetition-rate fs laser can generate changes in both real and imaginary parts of the permittivity, especially for long irradiation times or high laser pulse energies. Importantly, fs-written tracks in crystals possess a complex geometry and include volumes of material with increased and decreased RIs [6]. However, the change of RI, averaged across the cross section of each track, has always negative sign. Key parameters that were varied in the numerical model were extracted from experiments (the results will be published elsewhere). They include the track size d, the track spacing or pitch a, the RI contrast between the cladding and core regions δn, and the number of track rings or depressed-cladding layers N_r. On the other hand, in this work we did not explore different symmetries, more complex topologies or tiling, and disorder. Some of such examples can be found in [19].

$LiNbO_3$ is a class 3m, negative uniaxially birefringent crystal, suitable for both type I and type II (quasi-) phase matching [26]. In this study we considered a z-cut $LiNbO_3$ wafer, with the larger surfaces perpendicular to the z axis of the coordinate system, coincident with the optical axis of the crystal (Fig. 1). Light was assumed to propagate along the y axis. The Sellmeier expansions for the indices of 5 mol.% magnesium oxide (MgO) doped $LiNbO_3$ were taken from [27].

Maxwell's equations for monochromatic optical waves of angular frequency ω in a non-magnetic, anisotropic optical medium of relative permittivity $\hat{\varepsilon}$ yield the following wave equation for the electric field vector $\mathbf{E}$:

$$\nabla \times (\nabla \times \mathbf{E}) - \omega^2 \mu_0 \varepsilon_0 \hat{\varepsilon} \mathbf{E} = 0 \tag{1}$$

where ε_0 and μ_0 are the respective permittivity and magnetic permeability of a vacuum. The complex description is used for the electric field, and the time-dependence factor $\exp(i\omega t)$ is omitted. For a transparent, uniaxial crystal with the z optical axis, and hosting a depressed-cladding WG with the track RI contrast δn, the dielectric tensor can be written as

$$\hat{\varepsilon} = \begin{pmatrix} (n_o + \delta n)^2 & 0 & 0 \\ 0 & (n_o + \delta n)^2 & 0 \\ 0 & 0 & (n_e + \delta n)^2 \end{pmatrix} \tag{2}$$

where $n_{o,e}$ are the ordinary (O) and extraordinary (E) RIs of the intact domain of crystal, and δn is non-zero only in the irradiated domain. Given the direction of propagation along the y axis, a mode of propagation of the dielectric structure, that is, a solution of (1) with (2), is characterized by the mode's field pattern and its effective RIs $n_{o,e}^{\text{eff}} = \beta_{o,e}/k_0$, where $\beta_{o,e}$ is the propagation constant for x- and z-polarized light, respectively, and $k_0 = 2\pi/\lambda$ is the free-space wave number. Because of the finite transverse extent of the confining structure, the effective RI is a complex value; its imaginary part $\Im(n_{\text{eff}})$ is related to losses $\mathscr{L}$ (in decibels per centimeter) through the relation $\mathscr{L} = 40\pi\Im(n_{\text{eff}}) \times 10^4/[\lambda \ln(10)]$, where λ is given in micrometers. Dispersion parameter D is computed through the usual formula from the real part of effective RI $\Re(n_{\text{eff}})$ [28]: $D = -(\lambda/c)\partial^2\Re(n_{\text{eff}})/\partial\lambda^2$. Chromatic dispersion in micro-structured WGs arises from that of the unmodified material (D_{mat}) and also from the WG dispersion (D_W) associated with the structure of the confining region. Solution of Eqs. (1) and (2) provides directly the total dispersion (D), so we deduced D_W from the relation $D_W \simeq D - D_{\text{mat}}$.

#191696 - $15.00 USD Received 4 Jun 2013; revised 1 Jul 2013; accepted 2 Jul 2013; published 10 Jul 2013

Equations (1) and (2) were solved using the COMSOL simulation software based on the finite element method to find out the complex effective RIs $n_{o,e}^{\text{eff}}$ of the modes of the structure for the two orthogonal polarization states x and z. The wavelength was varied in the transparency window of 5% MgO-doped $LiNbO_3$. In the numerical simulations, a perfectly matched layer (PML) absorber was used to truncate the computational domain and, thus, minimize the effect of boundary reflections. We chose a circular PML surrounding the cross-section of the WG structure and isotropic in its absorption, defined by [29]

$$n_{\text{PML}}(r) = n_{o,e} - ik_{\max}\left(\frac{r-r_{\text{in}}}{L}\right)^2, \quad r_{\text{in}} < r \leq r_{\text{in}} + L \tag{3}$$

where r is the polar radial coordinate, r_{in} and L are the respective inner radius and thickness of the PML, and $k_{\max}$ is the maximum absorption value, which was assumed to be wavelength-independent. Special care was given to the choice of the parameters of the PML and the computational mesh. Indeed, the PML must have sufficiently large $k_{\max}$ to provide an adequate level of absorption and be wide enough to guarantee a small absorption gradient across its extent. In [30], the computational error was estimated to scale down with the PML's thickness approximately as $1/L^8$. The mesh size must be a few times smaller than the wavelength being used to ensure good accuracy of the results. In our simulations, we set $k_{\max} = 0.05$ and $L = 40\,\mu$m, and we mapped the computational domain with an automatically configured, triangle mesh with the minimum size $0.003\,\mu$m in the core of the domain and the relative growth rate 1.1. The maximum mesh size at the periphery of the domain was of the same order of magnitude as the shortest wavelength in use ($0.3\,\mu$m). The same mesh was used for all wavelengths in the range being studied. Optimized PML and mesh parameters led to a maximum error of approximately 10^{-10} dB/cm in the computed confinement losses $\mathscr{L}$. During the wavelength scanning, the most compact, Gaussian-like mode was selected using the criterium of 'minimum effective mode area'.

3. Results and discussion

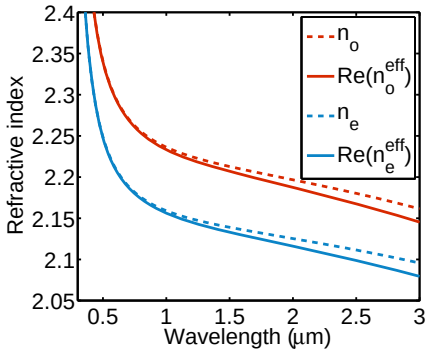

Fig. 2. Real parts of effective RIs for O and E waves as a function of wavelength for a depressed-cladding WG with two rings of tracks, $N_r = 2$. The O and E RIs of the unmodified material are also shown. WG parameters are: $d = 1.6\,\mu$m, $a = 2\,\mu$m, $\delta n = -0.05$.

One of the important features of micro-structured WGs is the control that their geometry and structural parameters can exert on the dispersion and loss characteristics of modes. The confinement losses that are intrinsically related to the WG geometry, in particular, are the most important parameter to consider in any practical design of WGs. In Fig. 2 we show a typical

#191696 - $15.00 USD Received 4 Jun 2013; revised 1 Jul 2013; accepted 2 Jul 2013; published 10 Jul 2013

evolution of the real parts of the effective RIs for the O and E waves with wavelength, for a depressed-cladding WG with two rings of tracks. In this example, we modeled tracks with the diameter $d = 1.6\,\mu$m and the pitch $a = 2\,\mu$m. Our recent fs inscription experiments in 5% MgO-doped $LiNbO_3$ (which will be described in a future work) have revealed that the track diameter may vary in the range from 1 to $3.5\,\mu$m. In the example of Fig. 2, the pitch was set to the minimum value ensuring no overlap of the tracks for the chosen track size. The induced RI contrast was $\delta n = -0.05$. This value is above the RI contrasts of the tracks of depressed-cladding WGs that can be achieved in 5% MgO-doped $LiNbO_3$ with current fs micro-fabrication technology – typical experimental values are around -0.01. However, since we have recently got experimental evidence that larger RI contrasts can in fact be obtained (the results will be published elsewhere), in a number of simulations we exceeded the value -0.01 to demonstrate the effect of higher RI contrasts on the waveguiding properties. It is seen from Fig. 2 that the deviation of the $\Re(n_{o,e}^{\rm eff})$ curves from the corresponding curves in the unmodified material $n_{o,e}$ becomes larger for longer wavelengths. This is an indication that with only two rings of tracks, the WG structure cannot confine the modes well at long wavelengths.

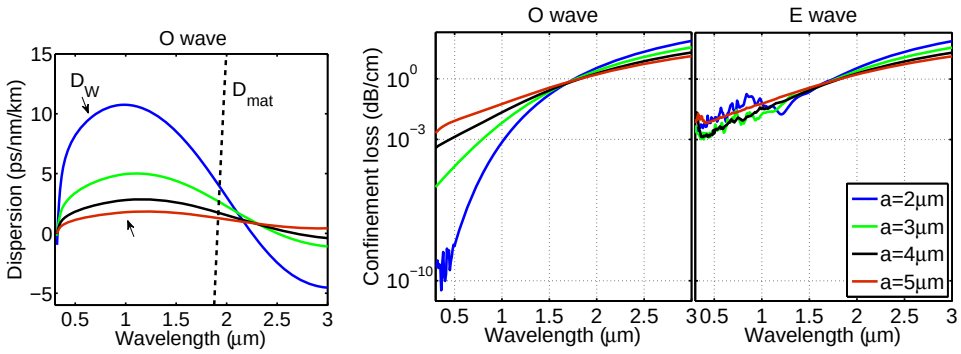

Fig. 3. Left: WG dispersion D_W for O wave, and right: confinement losses for O and E waves as a function of wavelength for a depressed-cladding WG with two rings of tracks with various pitches. The material dispersion $D_{\rm mat}$ is also shown. Other WG parameters are: $d = 1.6\,\mu$m, $\delta n = -0.05$.

In Fig. 3 we show the variation of the key WG quantities: WG dispersion D_W and confinement loss $\mathscr{L}$, as a function of both wavelength and track spacing for a WG with two rings of tracks. The pitch a was varied from 2 to $7\,\mu$m, whereas other WG parameters were kept the same as in Fig. 2. A noticeable trend in the dispersion curves is that the dispersion changes introduced by the WG are more pronounced for smaller a. These changes, however, are not big enough to affect the total dispersion of the structure significantly. Note that at the shorter wavelengths the depressed cladding can effectively confine the modes in the core guiding region. Guidance becomes worse at longer wavelengths, hence the modes behave like 'leaky modes'. Because of such a leakage at the longer wavelengths, none of the resonance features which would be expected due to the periodicity of the structure, can be observed. Moreover, band-gap resonances could be observed for this structure at wavelengths three or four times larger than the pitch, which fall outside the wavelength range used in our study. Our simulations also show that the change of the pitch in itself does not extend the spectral range where the loss figures for the modes are acceptably low. We assume here 1 dB/cm to be an acceptable loss level for technological applications.

The influence of the RI contrast of tracks on the WG dispersive and loss properties is illustrated by Fig. 4. There δn was varied from -0.02 to -0.05. It is clear that larger RI contrasts expand the wavelength region where the values of geometric loss are acceptably low, even with

#191696 - $15.00 USD Received 4 Jun 2013; revised 1 Jul 2013; accepted 2 Jul 2013; published 10 Jul 2013

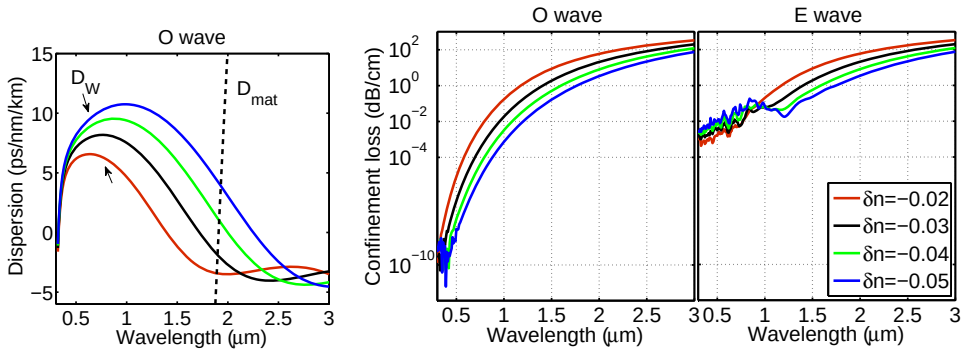

Fig. 4. Left: WG dispersion D_W for O wave, and right: confinement losses for O and E waves as a function of wavelength for a depressed-cladding WG with two rings of tracks of various RI contrasts. The material dispersion D_{mat} is also shown. Other WG parameters are: $d = 1.6\,\mu$m, $a = 2\,\mu$m.

only two rings of tracks. The wavelength region where the WG contribution to the total dispersion is not negligible becomes also wider, though the dispersion changes due to the WG remain small.

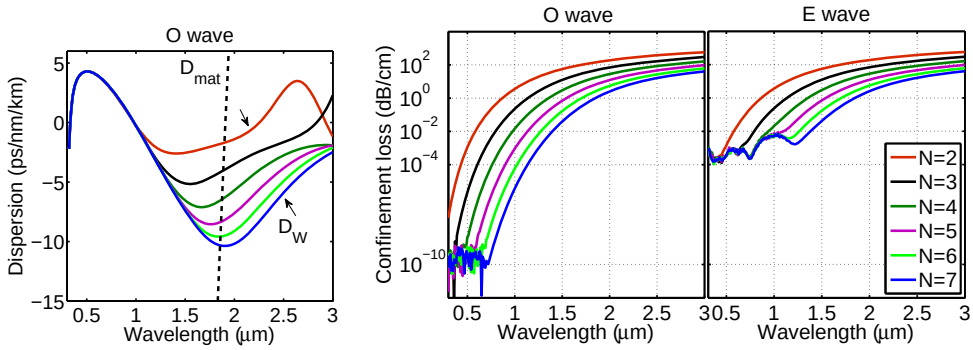

Fig. 5. Left: WG dispersion D_W for O wave, and right: confinement losses for O and E waves as a function of wavelength for a depressed-cladding WG with varying number of track rings. The material dispersion D_{mat} is also shown. Other WG parameters are: $d = 1.6\,\mu$m, $a = 2\,\mu$m, $\delta n = -0.01$.

A general fact that emerged from our study is that control over the waveguiding properties is better for compact cladding structures with small-sized and densely packed tracks with the largest possible RI contrasts. Figure 5 highlights the more interesting scenario that can be achieved with a varying number of cladding layers. The RI contrast was set to $\delta n = -0.01$ in these simulations. As can be seen from Fig. 5, while the dispersion changes due to the WG become increasingly more pronounced with increasing N_r, the overall effect of adding rings 3–7 on the dispersion properties of the structure is little. On the other hand, importantly, adding further rings of tracks can reach much better control over the losses even at the relatively moderate RI contrasts that are currently technologically feasible. As Fig. 5 shows, adding rings 3–7 results in an extension of the spectral range where the confinement losses in both O and E polarizations are below 1 dB/cm to the wavelengths near $2\,\mu$m, and in a reduction of the losses in both polarizations by more than three orders of magnitude near the telecommunication wavelength $\lambda = 1.55\,\mu$m. This is an important result for any practical applications of such

#191696 - $15.00 USD Received 4 Jun 2013; revised 1 Jul 2013; accepted 2 Jul 2013; published 10 Jul 2013

WG structures. We would like to note, however, that the figures reported here include only confinement losses showing the limitations that are due to the confinement by a micro-structured WG. In practice the total losses of the modes propagating in the structure will always be higher because of various factors, including: material absorption induced by fs irradiation, scattering losses due to irregularities (non-smoothness) of the cladding tracks, and imperfect positioning of the tracks which would increase the leakage of modes out of the guiding region.

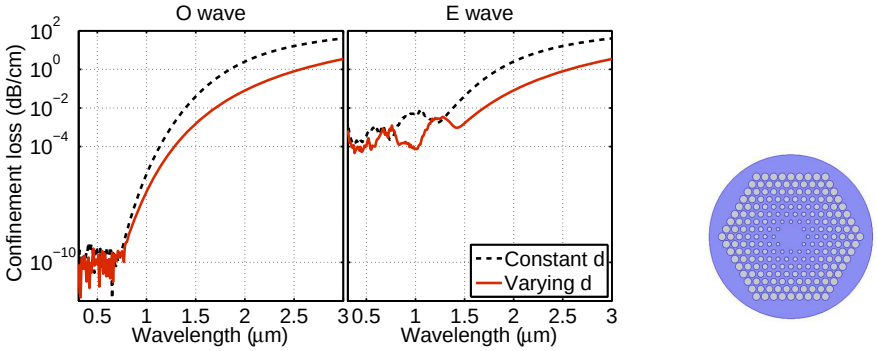

Fig. 6. Left: confinement losses for O and E waves as a function of wavelength for depressed-cladding WG with seven rings of tracks, $N_r = 7$, with different diameters $d = 1 - 2.2\,\mu$m. Other WG parameters are: $a = 2.5\,\mu$m, $\delta n = -0.01$. The losses for seven rings of identical diameter are also shown (extracted from Fig. 5). Right: cross section of modeled WG structure.

As it was shown by Renversez et al. [24] in the case of MOFs, a natural strategy to achieve low losses with fewer tracks or, equally, to extend the spectral range of low-loss operation of the WG structure, is to allow the track diameter to differ from one ring to another with the exterior rings that have large tracks. This design concept is illustrated in Fig. 6, which shows the variation of the confinement losses in the O and E polarizations with wavelength for a seven-ring structure with different track diameters. The track diameter of the innermost ring was arbitrarily set to $d_1 = 1\,\mu$m, and the diameter of subsequent rings was increased linearly up to the maximum value $d_7 = 2.2\,\mu$m for the outermost ring. Such a variation of the track size can be easily realized in practice by changing the energy of the irradiating fs laser pulses from one ring to another. Note, however, that this would entail a slight change in the induced RI contrast since also the latter depends on the pulse energy. The pitch was $a = 2.5\,\mu$m, and the RI contrast was $\delta n = -0.01$ in these simulations. One can see from Fig. 6 that, compared to the usual WG structure made of tracks of identical diameter (Fig. 5), this WG design allows us to expand the diapason of low-loss operation for both O and E polarizations into the mid-IR spectral region. Optimization of these WG geometries should enable further expansion of their low-loss operational spectral range.

An important issue that should be addressed here relates to the practical feasibility of the investigated WG structures. As mentioned previously, there are experimental limitations on the magnitude of the RI contrasts that can be reached for smooth tracks in crystals. Thus, to provide WG structures that display low-loss operation over a wide spectral range, the most viable solution is to write a fairly large number of rings of tracks, possibly with different sizes. These requirements on the number of rings make high-repetition-rate fs laser inscription the preferred micro-fabrication technique, as high-repetition-rate fs systems can enable up to four orders of magnitude quicker fabrication than the low-repetition-rate ones [15]. For example, for a propagation length of 10 centimeters in a WG with seven rings (around 200 tracks) the total length of the inscribed lines would amount to approximately 20 meters. Clearly, if one uses a

#191696 - $15.00 USD Received 4 Jun 2013; revised 1 Jul 2013; accepted 2 Jul 2013; published 10 Jul 2013

kHz fs system (with a typical sample translation speed of 10 to 100 μm/s, or of 500 μm/s by use of astigmatic beam inscription [16]), the fabrication time required on a single structure may exceed 60 hours, whereas a high-repetition-rate system can do the job in less than an hour.

4. Conclusions

We have shown numerically the feasibility of controlling the guiding properties of depressed-index cladding WGs that can be formed in a $LiNbO_3$ crystal by high-repetition-rate fs laser writing, by exploiting the WG geometric and structural characteristics. Our study ranged over the parameter space: track size, spacing, number of rings, and RI contrast, that is accessible experimentally. As we saw, the relatively moderate RI contrasts that are feasible by use of current fs micro-fabrication technology mean that geometric WG parameters have little control over the chromatic dispersion properties of the WG. On the other hand, the number of track rings revealed to play a major role in the control of the geometric losses. Importantly for technological applications, we have shown that for the typical induced RI contrast -0.01, increasing the number of rings from two to seven results in an extension of the spectral range where the confinement losses in both O and E polarizations are acceptably low (below 1 dB/cm) to the wavelengths near 2 μm, and in a reduction of the losses in both polarizations by more than three orders of magnitude near the telecommunication wavelength $\lambda = 1.55\,\mu$m. We have also shown that WG designs with track diameters that differ from one ring to another [24] can further expand the spectral region of low-loss operation into the mid-IR range. Similarly, these designs would allow us to achieve low losses with fewer tracks. In view of the requirements imposed by losses on the number of rings, high-repetition-rate fs lasers would advantageously be used to fabricate the WG structures studied in this paper. We plan to develop optimization procedures and design principles for micro-structured WGs in $LiNbO_3$ that are tailored to specific applications in a future work.

Acknowledgments

We would like to thank Dr. Vladimir Mezentsev, Prof. Keith Blow (Aston University) and Prof. Ivan Avrutsky (Wayne State University, Detroit, MI, USA) for fruitful discussions. We also acknowledge support from the Leverhulme Trust (grant RPG-278).

#191696 - $15.00 USD Received 4 Jun 2013; revised 1 Jul 2013; accepted 2 Jul 2013; published 10 Jul 2013